

GAUSSIAN DECOMPOSITION OF H I SURVEYS – II. SEPARATION OF PROBLEMATIC GAUSSIANS

U. Haud¹ P. M. W. Kalberla²

¹ *Tartu Observatory, EE61602 Tõravere, Tartumaa, Estonia*

² *Radioastronomisches Institut der Universität Bonn, Auf dem Hügel 71, 53121 Bonn, Germany*

Received November 5, 2018; revised November 5, 2018

Abstract. We have analyzed the results of the Gaussian decomposition of the Leiden/Dwingeloo Survey (LDS) of galactic neutral hydrogen for the presence of Gaussians probably not directly related to galactic H I emission. It is demonstrated that at least three classes of such components can be distinguished. The narrowest Gaussians, obtained during the decomposition, mostly represent stronger random noise peaks in profiles and some still uncorrected radio-interferences. Many of slightly wider weak Gaussians are caused by increased uncertainties near the profile edges and with the still increasing width the baseline problems become dominating among weak components. Statistical criteria are given for separation of the parameter space regions of the Gaussians, most likely populated with the problematic components from those where the Gaussians are with higher probability describing the actual Milky Way H I emission.

The same analysis is applied also to the Leiden/Argentina/Bonn survey (LAB), a compilation that combines a revised version of the LDS (LDS2) with the stray radiation corrected version of the Southern sky survey of the Instituto Argentino de Radioastronomía (IAR). It is demonstrated that the selection criteria for dividing the parameter space are to a great extent independent of the particular survey in use. The situation is more obscure for very wide components. In this region the distributions of the components of different origin seem to be more blended and it is harder to decide on the basis of Gaussian parameters alone, whether the corresponding components are caused by some high velocity dispersion halo gas in the Milky Way, external galaxies or are due to baseline problems, for example. Nevertheless, the presence of the baseline problems in the LDS is most likely indicated by the peculiarities of the distribution of the widest Gaussians in the sky. A similar plot for the northern part of the LAB demonstrates considerably lower numbers of spurious components, but there are still problems with the southern part of the LAB. The strange characteristics of the observational noise in the southern part of the LAB are also pointed out.

Key words: Methods: data analysis – Surveys – Radio lines: ISM

1. INTRODUCTION

The Gaussian analysis of the observed HI profiles is a somewhat controversial process. On the one hand, if we neglect the saturation and absorption effects, suppose that most of the line shape comes from global rotation characteristics of the Galaxy and that the galactic HI consists of separate hydrogen clouds with equilibrium random velocity distribution, the observed profile can be considered as a sum of Gaussian cloud components, shifted relative to each other by differential rotation.

Unfortunately, the actual situation is much more complicated. We must consider the possibility of intrinsically non-Gaussian contributions to the emission (due to groups of atoms with asymmetrical or in any other way pronounced non-Gaussian velocity distribution or due to saturation in optically thick regions and self-absorption by very cold foreground gas). Except for the simplest profiles, the least squares Gaussian analysis is not unique (often several quite different solutions may fit the observations almost equally well, and the method of the least squares provides no satisfactory means for choosing between these solutions, while other, equally good or even better ones, may not be found at all). Strictly speaking, the pure method of the least squares is even not valid, when applied to this problem, as neither the form of the components nor their number is known, nor can it be assumed that the residuals are randomly distributed. The solution is often partially determined by the number of components introduced, the initial estimates of their parameters and only partially by the observed profile. All this makes a rigorous Gaussian analysis somewhat illusive.

These weaknesses of the Gaussian analysis were understood rather early (Kaper et al. 1966; Takakubo & van Woerden 1966). Nevertheless, the method continued to be used up to the present time (e.g. Cappa de Nicolau & Pöppel 1986; Pöppel et al. 1994; Verschuur & Peratt 1999; Verschuur 2004). This indicates that besides weaknesses the method must have also some benefits (some aspects briefly discussed in Sec. 2.2 and in Haud 2000, hereafter Paper I). Proceeding from this, we have created a new fully automatic specialized computer program for the decomposition of large 21-cm HI line surveys into Gaussian components. This program has been described in Paper I and it represents the profiles as formal sums of only positive Gaussian functions without considering the actual line formation processes. During the decomposition process the special attention is paid to the following features:

1. Several quite different solutions may often fit the observations almost equally well. To choose from these solutions, it was supposed that general properties of the hydrogen distribution are somewhat correlated at neighboring sky positions and therefore the program tries to find similar decompositions for corresponding profiles.
2. With the increasing complexity of the observed profiles, the number of Gaussians in decompositions usually grows rapidly and the values of their parameters become mutually dependent. To reduce this problem, special means have been used to keep the number of Gaussians as small as possible.

In this paper we describe the first results from the application of the new decomposition program on the Leiden/Dwingeloo Survey of galactic neutral hydrogen by Hartmann & Burton (1997, hereafter the LDS) and on the recent Leiden/Argentine/Bonn compilation of galactic HI results by Kalberla et al. (2005,

hereafter the LAB). We start with the description of the data used, the results obtained and possible approaches to the interpretation of the decomposition results (Section 2) and then proceed with the analysis of the results for the LDS (Section 3) and the LAB (Section 4). In this analysis, the main attention is paid to the separation of the features, most likely corresponding to the real emission of galactic HI, from those representing different problems during observations, reduction and decomposition of the surveys. Such a separation may be important at least in two aspects. On the one hand, such separation may help us to identify the problems with the observational data; on the other hand, it may give us a cleaner sample of Gaussians for studying the properties of the Milky Way HI. At the same time, it is important to understand that the discrimination between different Gaussians, as described in this paper, is statistical in its nature and as the distributions of different types of Gaussians partially overlap, it cannot be used as the only and final criterion for every particular Gaussian or profile.

In the present paper, we turn our main attention to the minority of the Gaussians, most likely describing different types of problems, which could be searched for using the components, recognized as probably suspicious. In the further papers we will continue the study of the majority of the Gaussians, which may with higher probability measure the spectral signatures of higher astronomical interest.

2. INTERPRETATION OF THE DECOMPOSITION RESULTS

2.1. The data

As test data for our decomposition program we used the original observed profiles of the LDS (Hartmann 1994), reduced to T_b by P. M. W. Kalberla at Bonn University (the reduction procedures described in Hartmann 1994 and Hartmann et al. 1996). These are not exactly the same as those published by Hartmann & Burton (1997) on a CD-ROM. We have used the profiles before averaging the repeated observations at identical sky positions and before re-gridding them onto a common lattice. This choice was made, as averaging and re-gridding smear the differences between neighboring profiles and may have undesirable influence on the Gaussian decomposition process (see Introduction of Paper I). In this original form the survey contained 184 698 profiles, which after decomposition were represented by 1 493 187 Gaussians. For a brief comparison also 206 671 profiles of the published version of the LDS were decomposed into 1 644 665 Gaussians.

Recently a similar Southern sky high sensitivity HI survey at $\delta \leq -25^\circ$ was published by Bajaja et al. (2005) (IAR). IAR and the LDS with the revised stray-radiation and baseline corrections (LDS2) make up the LAB. The specifications for LDS2 and IAR closely match each other, but all the data reduction and calibration procedures were carried out entirely independently for both of the surveys. Proceeding from this, also the Gaussian decomposition was carried out separately for the LDS2 and the IAR. Once again, the original data were used for both surveys. As for the LDS2 the repeated observations were not averaged any more, but the final profiles were selected on the basis of the best agreement of their Gaussian decompositions with the decompositions of the neighboring profiles, we used these preselected profiles for the analysis. In the case of the IAR, we first used for the decomposition the original 1008-channel data of all observed profiles and for

repeated observations we applied the same selection criteria as used for the LDS2. This procedure gave us 1 064 808 Gaussians per 138 830 profiles for the LDS2 and 444 573 Gaussians per 50 980 profiles in the case of the IAR.

2.2. The usage of Gaussians

In general, the results of these Gaussian decompositions may be interpreted from two completely different points of view:

1. Gaussian parameters may be considered just as a compact means for representing the observed data without providing any physical interpretation to these parameters, or
2. we may want to derive from the parameters of the obtained Gaussians direct information regarding the structure of the interstellar medium.

For the first purpose, even in the case of the most complicated profiles, hundreds of channel values in the profile are replaced by some tens of Gaussian components, while physically significant information, such as mean velocities and the HI content of the HI features, can still be as easily extracted as from full profile data (Shane 1971). If correctly performed, the decomposition just discards observational noise and in this case we must consider all obtained Gaussians as real as the original profile data and the criteria for performing the decomposition. Moreover, usually some specific features in the observed profiles (not necessarily corresponding to some distinct gas clouds in physical space) are represented by some specific set of Gaussians, which can be found from the overall data-set more easily than un-parameterized spectral features. As noted by Verschuur & Peratt (1999), such Gaussian analysis allows us to characterize general properties of the profiles from region to region in the sky and to draw conclusions, based upon similarities and differences in profile shapes. Verschuur has used this approach to study the relations between the different line-width regimes of the HI in the local interstellar medium and the critical ionization phenomenon (Verschuur & Schmelz 1989; Verschuur & Magnani 1994; Verschuur & Peratt 1999; Verschuur 2004). This is also the way of interpretation used in the present paper. We are looking for patterns in the distribution of Gaussians, corresponding to different problems in the obtained decomposition.

The second approach is much more complicated as it is well known that Gaussians may yield direct information regarding the structure of the interstellar medium only for the simplest profiles, where at least some Gaussians are well separated. This considerably reduces the usefulness of the Gaussian decomposition in directions close to the galactic equator, where the line of sight may contain hundreds of times more gas than at higher latitudes. The situation could not be improved even by increasing the resolution of observations, as the shape of the emission spectra does not change greatly with angular resolution (Baker & Burton 1979). This is so because near the galactic plane the more or less continuous distribution of HI extends to distances much larger than at high latitudes and the velocity crowding squashes a lot of space into a few kilometers per second. Individual interstellar components blend completely, and little structure is revealed by increasing the resolution. Only when an emission feature has a very odd velocity or is considerably brighter than its surroundings, so that it is not blended by other emission, the Gaussian analysis may still provide some information on the

properties of the interstellar gas (limits on velocity dispersion and temperature, for example). Due to these considerations, we first use for our discussions only the decomposition results obtained for relatively high galactic latitudes ($|b| \geq 30^\circ$), but afterwards we test also how much and in what general properties of the decomposition results differ for the regions near the galactic plane and farther away.

However, even if we consider only relatively simple profiles at high galactic latitudes, some of the well separated Gaussians, obtained during the decomposition process, may correspond to other features in profiles than the real emission from galactic HI. Therefore, when in an ideal case, the Gaussian analysis can be used to separate the useful signal from the observational noise, in reality such a separation is never perfect. For example, some Gaussians obtained may still represent the inaccuracies in the termination criteria of the decomposition process, when stronger noise peaks are still fitted by Gaussians (actually, for our program these criteria were deliberately chosen in the way preferring fitting of some noise to losing a weak signal – see Paper I), or suspicious features (radio-interferences, bad baseline and so on) contained in profiles themselves. Proceeding from this, the main focus of this paper is on the question, whether it is somehow possible to separate such Gaussians from other, physically more founded ones, and in this way to further clean the decomposition results. As a working hypothesis, we expect that the distributions of the parameter values of the Gaussians, representing different artifacts, may be distinguishable from those of the Gaussians corresponding to the real HI emission of the Milky Way and it may be possible to isolate the regions of the parameter space dominated by components of one or another origin.

3. LDS

3.1. Narrow Gaussians

For separation of different kinds of Gaussians their distribution in the plane of height and width seems to be most informative. The height of a Gaussian is defined by the value of the central brightness temperature $T_{b0} > 0$ from the standard Gaussian formula

$$T_b = T_{b0} e^{-\frac{(v-V_C)^2}{2\sigma^2 V}}, \quad (1)$$

where T_b is the brightness temperature and V is the velocity of the gas relative to the Local Standard of Rest. V_C is the velocity corresponding to the center of the Gaussian. We characterize the widths of the components by their full width

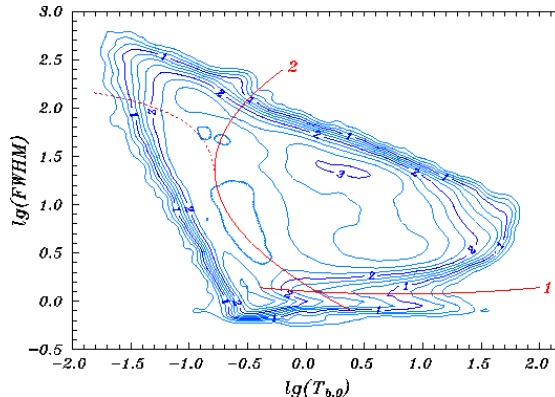


Fig. 1. Frequency distribution of the parameter values in $(\lg(T_{b0}), \lg(\text{FWHM}))$ plane for all Gaussians, corresponding to profiles at galactic latitudes $|b| \geq 30^\circ$. Isodensity lines are drawn in the scale of $\lg(N+1)$ with the interval of 0.25. The thick solid and dashed red lines represent the selection criteria discussed in the text.

at the level of half maximum (FWHM), which is related to the velocity dispersion σ_V by a simple scaling relation $\text{FWHM} = \sqrt{8 \ln 2} \sigma_V$.

To avoid the complicated profiles near the galactic plane, we present in Fig. 1 the $(\lg(T_{b0}), \lg(\text{FWHM}))$ distribution of all Gaussians for the LDS profiles at galactic latitudes $|b| \geq 30^\circ$. From this figure we can see that most frequently the Gaussians have the heights between about $1 \lesssim T_{b0} \lesssim 10$ K and widths $3 \lesssim \text{FWHM} \lesssim 30$ km s⁻¹. These parameters are in general agreement with the usual two-phase models of the atomic interstellar medium, where one phase is cold with temperatures of about 100 K (CNM) and the other is warm with temperatures of several thousands degrees (WNM). Considering also the temperature variations and the additional line broadening due to the macroscopic turbulent motions in the interstellar structures ($\sigma_V \simeq 2-5$ km s⁻¹ according to Burton 1992), the widths of corresponding H I emission lines are in the range of about $1 \lesssim \text{FWHM} \lesssim 10$ km s⁻¹ for CNM (Crovisier 1981) and $12 \lesssim \text{FWHM} \lesssim 40$ km s⁻¹ for WNM (Mebold 1972). There are, however, concentrations of Gaussians also around $\lg(T_{b0}) \approx -0.4$, $\lg(\text{FWHM}) \approx 0$ and $\lg(T_{b0}) \approx -0.9$, $\lg(\text{FWHM}) \approx 2.1$.

The first of these concentrations extends from relatively weak Gaussians up to the intensities of several tens of kelvins, and the widths are mostly below the limit corresponding to the kinetic temperature of the coldest H I observed (Verschuur & Knapp 1971, 1972; Braun & Burton 2000). Therefore, it is likely that these components are not directly related to the emission of the galactic gas, but represent some artifacts of the profiles or their Gaussian decomposition process. An inspection of corresponding profiles confirms this guess. In Fig. 2 two examples are given. The upper panel represents a H I profile, measured at $l = 228.9^\circ$, $b = 54.5^\circ$ and decomposed into 17 Gaussians of which 13 have widths around 1 km s⁻¹. One of these narrow Gaussians is rather strong with the height of nearly 19 K,

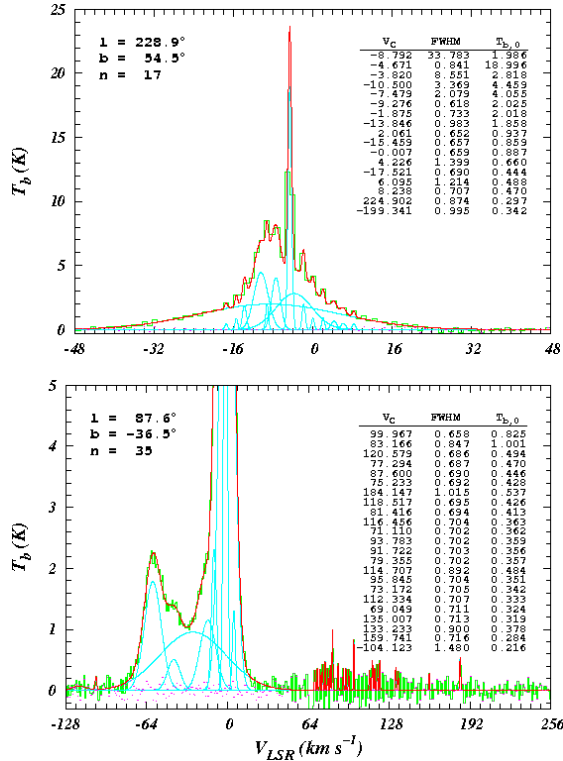


Fig. 2. Two examples of the profile with very narrow Gaussians. The observed profiles are plotted with the stepped green lines, individual Gaussian components with the thin smooth cyan lines, the Gaussian representation of the profiles with the thick smooth red lines and the residuals with small magenta points. Due to the large number of Gaussians in lower panel only the parameters of very narrow components are given.

representing the central peak of the typical radio-interference, and most of the other Gaussians fit the fading oscillations on both sides of the central peak. There are also two narrow Gaussians (not shown in Fig. 2) at higher velocities, which represent some stronger noise peaks, not directly related to the illustrated interference pattern. The lower panel illustrates the Gaussians fitting the noise peaks. As the noise level at the velocities around 100 km s^{-1} is higher (probably due to the corrected radio-interference) than in other regions of the profile, this higher noise have brought about a large number of spurious Gaussians.

As the described very narrow Gaussians are separated in Fig. 1 from the distribution of the wider ones by a clearly visible “valley” of relatively underrepresented values of Gaussian parameters, it seems rather safe to draw the separation line between the Gaussians describing the emission of the galactic HI and those representing the noise and radio-interferences, along the bottom of this valley (line 1 in Fig. 1). To select the shape and placement of this line, we first counted the Gaussians in (0.05×0.05) bins in $\lg(T_{b0})$ and $\lg(\text{FWHM})$, found for every strip of $-0.3 \leq \lg(T_{b0}) \leq 1.2$ the value of $\lg(\text{FWHM})$, corresponding to the bin with the smallest number of Gaussians and fitted the parabola through the obtained $(\lg(T_{b0}), \lg(\text{FWHM}))$ pairs. Finally, the parameters of the parabola were adjusted by demanding that the sum of the numbers of Gaussians in the bins, through which the parabola is drawn, should be minimal. In some approximation the result,

$$\lg(\text{FWHM}) = 0.046 * \lg(T_{b0})^2 - 0.074 * \lg(T_{b0}) + 0.104, \quad (2)$$

could be used as a selection criterion to separate the Gaussians representing interferences and noise peaks from those describing the properties of the emission of the galactic HI.

3.2. Weak Gaussians of intermediate widths

Around $\lg(T_{b0}) \approx 0$ and $\lg(\text{FWHM}) \approx 0$ the valley in Fig. 1 turns towards the wider Gaussians, broadens and becomes less deep. Therefore, it is interesting to check, if here also the region of underrepresented values of Gaussian parameters may help us to separate the components describing different phenomena. The answer seems to be yes. It is known that the receiver bandpass is never square. As a result, the extreme edges of the obtained spectra are steeply falling off to zero intensity and after the bandpass removal the intensities in these channels become unreliable due to the division by reference. Moreover, the usual methods of baseline fitting are poorly constrained in these regions. To take this into account, during the decomposition we have not used

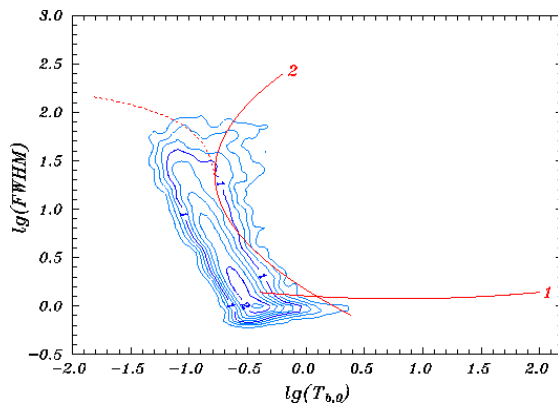


Fig. 3. The frequency distribution of the parameters of the Gaussians near the profile edges. The designation is the same as in Fig. 1.

the data from 64 channels with the most negative velocities and from 128 channels with the highest positive velocities. However, the excess noise and baseline problems at the edges of the reduced profiles are not confined by sharply defined velocity ranges. In some profiles they can be detected in wider regions, in other profiles in more limited regions. To study how this is expressed in the “language” of Gaussians, we plot in Fig. 3 the distribution of the Gaussians, which have central velocities closer to the accepted profile ends than 64 channels. We can see that these Gaussians populate the region separated in Fig. 1 from the main body of the distribution by the valley running towards the upper left-hand corner of the plot.

In Fig. 4 two examples are given. The upper panel gives the HI profile, measured at $l = 211.5^\circ$, $b = 17.0^\circ$ and decomposed into 12 Gaussians, 4 of which have central velocities higher than 330 km s^{-1} – the velocity limit, corresponding to the 192th channel from the positive velocity edge of the observed profile. We can see that at these extreme velocities the baseline has been drawn too low, causing the resulting mean profile to arise above the zero intensity level. In the Gaussian decomposition this behavior is expressed by adding a rather weak ($T_{b0} \approx 0.05 \text{ K}$) but broad component with $\text{FWHM} \approx 83 \text{ km s}^{-1}$. The profile also becomes wavy in this region. As a result, the decomposition program adds two more weak Gaussians at velocities $V_C \approx 333 \text{ km s}^{-1}$ and 375 km s^{-1} . Finally, as the program has considered the increase of the profile mean channel values at extreme velocities as a sign of presence of a possible useful signal, the actual noise level of the profile is underestimated. As the decomposition program tries to reduce the level of residuals to the value near the estimated noise level of the profile, this results in several very narrow Gaussians, representing the strongest noise peaks all over the profile.

The narrow Gaussians in Fig. 4 could be detected and rejected from the obtained Gaussian representation of the LDS using the selection criterion 1 (Eq. 2) discussed above. As demonstrated by Fig. 3, the wider Gaussians near the profile edges in Fig. 4 fall to the left of the region of underrepresented values of the Gaussian parameters in Fig. 1. Therefore, it seems plausible that even after

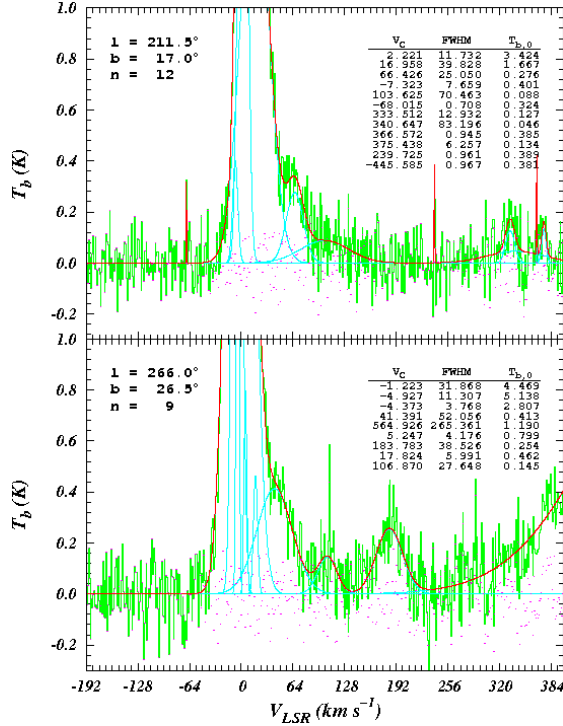


Fig. 4. Two examples of the profiles with the problems at the positive velocity edge. The notation is the same as in Fig. 2.

the valley in the distribution of the Gaussian parameters in Fig. 1, turns up near $\lg(T_{b0}) \approx 0$ and $\lg(\text{FWHM}) \approx 0$, it still may be interpreted as the division between Gaussians, representing the actual emission of the galactic HI and those describing the observational, reductional and decompositional problems. On the basis of these considerations, we followed the underpopulated region to even wider Gaussians and approximated the run of the location of the most sparsely populated parameter values with the parabolic curve (solid line 2 in Figs. 1 and 3).

However, in Fig. 3 we can also see that in the region of the widest Gaussians a considerable fraction of them fall to the right of the parabolic curve, determined from the location of the distribution minimum in Fig. 1. A closer inspection of the situation indicates that the majority of these Gaussians have central velocities outside the range of channels, actually used in the decomposition process. That means, they are similar to the $\text{FWHM} \approx 83 \text{ km s}^{-1}$ Gaussian in Fig. 4, but with its center not at $V_C \approx 340 \text{ km s}^{-1}$, but shifted beyond the right border of the figure. These Gaussians arise in the cases where the baseline has been drawn progressively lower and lower towards the end of the used velocity range and the resulting profile continues to rise higher and higher above the zero level when approaching the velocity limit of the profile, as illustrated in the lower panel of Fig. 4. The parameters of such Gaussians are poorly determined as they are estimated from the relatively small number of profile channels, covering less than a half of the full extent of the component. These Gaussians could be easily recognized by demanding that all the accepted components must have their central velocities inside the velocity range, used for decomposition.

3.3. The broadest Gaussians

We have determined the shape and location of curve 2 in Fig. 3 in the same way as described for curve 1. However, when at lower values of FWHM curve 2 can be rather easily determined from the data used for Fig. 1, this becomes increasingly uncertain when moving to higher values of FWHM. Above $\lg(\text{FWHM}) \approx 1.35$ the valley bifurcates and the curve may actually follow even two completely different passages: the one indicated in Fig. 1 with the solid line, or the other one, indicated by the dashed line. The main difference between these two possibilities is that in the first case the widest Gaussians, obtained during the decomposition, are excluded from the region corresponding to the components representing the actual emission of the galactic HI, and in the second case, they are included in this region. Therefore, it is important to know what is actually represented by such Gaussians.

Some decades ago, Field et al. (1969) demonstrated that the HI could be considered as a two-phase medium, where much of the gas is observed to be either WNM with $T \sim 10^4 \text{ K}$ or CNM with $T \sim 100 \text{ K}$ (Kulkarni & Heiles 1987; Dickey & Lockman 1990). These temperatures correspond to line-widths mostly below 21 km s^{-1} and the corresponding Gaussians have $\lg(\text{FWHM}) \lesssim 1.9$ even if we allow for realistic turbulent motions in the gas (Mebold et al. 1982; Kulkarni & Fich 1985). Kalberla et al. (1998) have argued in favor of the existence of some neutral gas with velocity dispersion as high as $60 - 80 \text{ km s}^{-1}$ in the halo. The Gaussians, corresponding to such gas may have $\lg(\text{FWHM}) \lesssim 2.3$, the limit still considerably below the highest values of $\lg(\text{FWHM})$ in Fig. 1. Therefore, it seems clear that the widest Gaussians in Fig. 1 cannot be interpreted as the representation of the real HI emission and this favors the solid line 2 as a selection criterion.

However, what is then represented by the widest Gaussians rejected by the second selection criterion? To discuss this, we first turn to the distribution of the weak Gaussians, remaining to the left of the solid curve 2 in Fig. 1, in the central velocity – line-width plane (Fig. 5). Here we can see that the widest Gaussians are concentrated in their velocities mainly around the value of $V_C = 0 \text{ km s}^{-1}$ with the distribution extending to slightly more than 150 km s^{-1} at both sides. Less prominent concentrations of wide Gaussians are at higher velocities (approximately at $-390 \lesssim V_C \lesssim -230 \text{ km s}^{-1}$ and $180 \lesssim V_C \lesssim 280 \text{ km s}^{-1}$). There is a certain excess of wide Gaussians also near the profile edges, but we have already discussed them above.

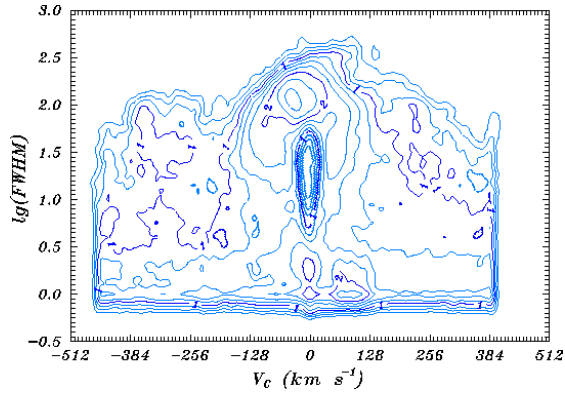


Fig. 5. The distribution of the weakest Gaussians (those remaining to the left of the solid curve 2 in Fig. 1) in the central velocity – line-width plane. The isodensity lines are drawn in the scale of $\lg(N + 1)$ with the interval of 0.25.

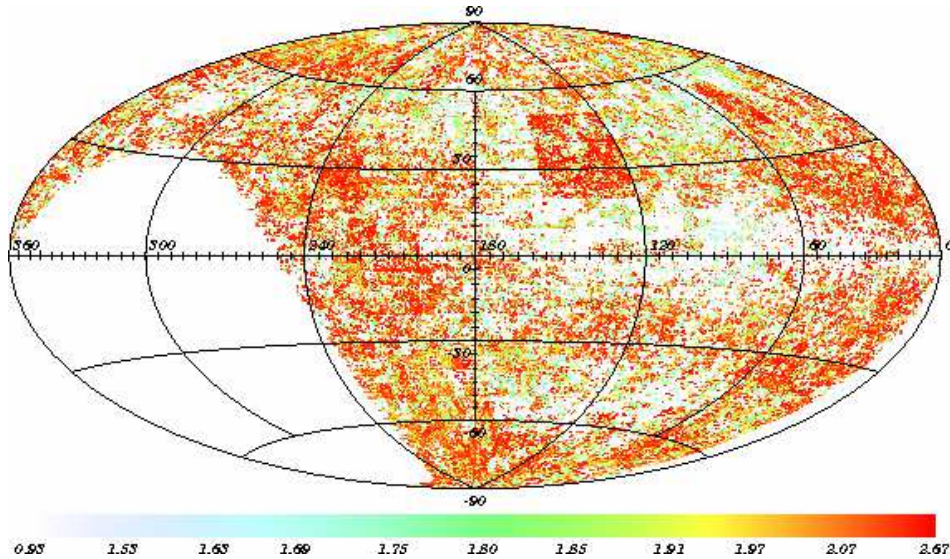


Fig. 6. The sky distribution of the widest weak Gaussians in galactic coordinates. The color-scale represents the width (in units of $\lg(\text{FWHM})$) of the widest Gaussian obtained for a given sky position and the gradation is chosen to enhance the contrast of quadrangular fields.

In Fig. 6 we present the sky distribution of the Gaussians of the concentration near the zero velocity in Fig. 5 (velocities $-152 \lesssim V_C \lesssim 160 \text{ km s}^{-1}$). We can see that in surprisingly many places (best visible at $l > 180^\circ$ and $b < -30^\circ$)

these components form quadrangular “clouds” in the sky (a similar pattern is not visible if we use the Gaussians lying to the right of the solid curve 2 in Fig. 1). The size of these clouds is often $5 \times 5^\circ$ or an integer multiple of this. If we recall now that the LDS observations were made by $5 \times 5^\circ$ fields and the same fields were involved also in bandpass removal (Hartmann 1994), it seems that at least a considerable number of wide Gaussians must be due to some observational or reductional problems specific to each $5 \times 5^\circ$ field and cannot describe the actual properties of galactic HI. This is the main justification for choosing the second selection criterion as indicated by the solid line 2 in Fig. 1, corresponding to

$$\lg(T_{b0}) = 0.547 * \lg(\text{FWHM})^2 - 1.492 * \lg(\text{FWHM}) + 0.235. \quad (3)$$

3.4. The high velocity dispersion halo gas

When constructing Fig. 6, we tried several versions of the color-scale to find the one, which enhances most the contrast of the quadrangular structures. We found that this pattern is dominating among the Gaussians with widths above $\lg(\text{FWHM}) \gtrsim 1.8$, a result in good agreement with Fig. 5, where we can see that the concentration of very wide Gaussians around zero velocity extends down to the widths $\lg(\text{FWHM}) \gtrsim 1.8$. At the same time, if to draw a figure similar to Fig. 6, but for wide Gaussians at velocity intervals $-390 < V_C < -230 \text{ km s}^{-1}$ and $180 < V_C < 280 \text{ km s}^{-1}$, we cannot see the quadrangular pattern as in Fig. 6 and the picture is dominated by two concentrations of points, clearly coinciding in location and shape with the northern tip of the Magellanic Stream and the high-velocity cloud (HVC) complex AC. Therefore, it seems that not all wide Gaussians rejected by the selection criterion of Eq. (3), are due to observational or reductional problems, but some of them correspond to real gas.

Moreover, at this level of discussion it remains unclear if and how Gaussians represent the high velocity dispersion halo gas (HVDHG) discussed by Kalberla et al. (1998). From their Fig. 1 we may estimate that corresponding Gaussians, if

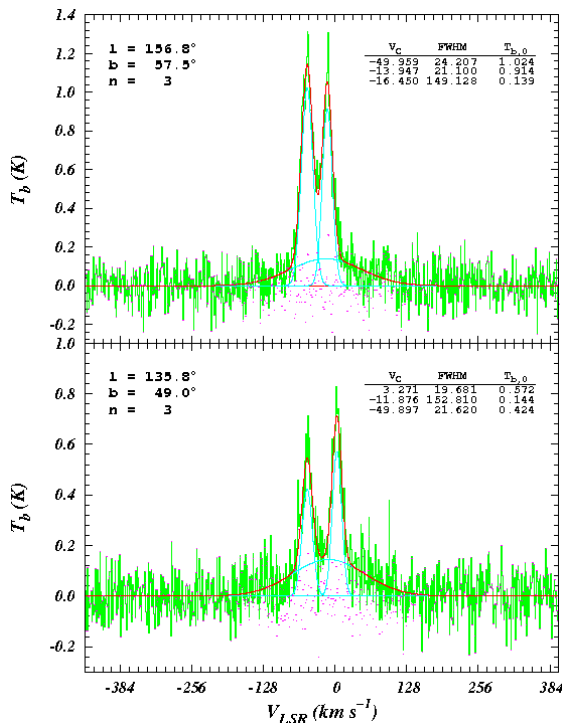


Fig. 7. The examples of the profiles with broad Gaussians. The cases represented in the upper and lower panel are discussed in the text. The notation is the same as in Fig. 2.

present in our decomposition, must have the heights of the order of $T_{b0} \approx 0.05$ K. In our Fig. 1 they lie to the left of the solid line 2 and would be rejected by the brute force application of the second selection criterion. We postpone the detailed discussion of this question to further papers, but we point out here that we believe that our decomposition has detected such gas. Most likely the corresponding Gaussians may add somewhat to the concentration around $V_C = -30 \text{ km s}^{-1}$, $\lg(\text{FWHM}) = 2.2$ in Fig. 5 and form part of the more diffuse background in Fig. 6. Nevertheless, it is clear that most of the widest Gaussians in Fig. 1 do not represent the properties of the real gas, but it is harder to draw a clear cut separation line between different types of Gaussians in this region than at smaller widths. In such a separation process we cannot rely only on heights and widths of Gaussians, but we must also consider at least their velocities.

Actually it is as hard to classify corresponding Gaussians as to decide when the broad wings of the HI emission lines in the observed profiles represent the HVDHG and when they are caused by some problems, most likely the badly behaving baselines or stray-radiation corrections. We illustrate this in Fig. 7, where the profile in the upper panel is selected from the light $5 \times 5^\circ$ field in Fig. 6 (the median width of the widest Gaussians of every point of the field is equal to 19.7 km s^{-1}) and the profile in the lower panel from the dark one (the median equals to 187 km s^{-1}). In this way we may expect that the profile in the lower panel probably has its widest Gaussian due to baseline problems and in the upper panel the widest Gaussian is more likely caused by HVDHG. However, the widest Gaussians in both panels have nearly the same widths and intensities and also the general shapes of the profiles seem to be rather similar.

From the observed profile in the upper panel of Fig. 7 it may seem that the decomposition with 4 Gaussians (with parameters given in Table 1) may give a better model with more realistic widths of Gaussians. A closer inspection does not confirm this expectation. Before decomposition the noise level of the signal-free regions of this profile was estimated to be equal to 0.0864 K. If we divide the profile into two regions, where the total intensity of the obtained Gaussians is below 10% of this noise level (signal-free region) and above 10% of the noise level (the region with signal), we can compute in both regions the rms of residuals after subtracting the obtained Gaussians from the observed profile. In the case of a three component fit the corresponding numbers are 0.0865 K and 0.0864 K, respectively. We see that this model identifies nearly equal noise levels in both regions of the profile – a result we should expect (by applying corresponding weights we have taken into account the dependence of the noise on signal strength, as described in Paper I). For a four component fit we receive 0.0871 K and 0.0790 K, clearly indicating that we have used too many Gaussians and made the rms of the residuals in the region containing the signal, too low.

Therefore, on the basis of the present discussion, we cannot determine unambiguously the reason for the broad Gaussians. Some of them may correspond to real HI emission, others to artifacts due to the problems in baseline determination. However, even for wide Gaussians Figs. 1, 5 and 6 may help us separate

Table 1. A four-component fit.

V_C	FWHM	T_{b0}
-51.994	18.660	0.780
-13.770	12.198	0.705
-28.634	71.642	0.517
83.636	36.210	0.087

the regions of the parameter space, where such problems exist, from those, where most components with high probability describe the real emission.

3.5. Low galactic latitudes and the Atlas

So far we have discussed mainly the data for the regions at $|b| \geq 30^\circ$, where the hydrogen profiles are simpler than near the galactic plane. At the same time, we have pointed out that the Gaussian analysis allows us to characterize general properties of the profiles from region to region in the sky and to draw conclusions based upon similarities and differences in profile shapes. Therefore, it is interesting to check how different the $(\lg(T_{b0}), \lg(\text{FWHM}))$ distribution of Gaussians at low galactic latitudes is in comparison to Fig. 1. The corresponding results are presented in Fig. 8. We can see that the main difference between Figs. 1 and 8 is a greater extent of the distribution towards the stronger and wider Gaussians in Fig. 8. This means that at low galactic latitudes many Gaussians are higher and/or wider than at high latitudes – the property caused by a complex superposition of low optical density gas in and near the galactic plane, which could not allow us to distinguish in many cases the contribution of every single concentration of HI.

However, despite the presence of large numbers of Gaussians, representing the total emission of unknown numbers of actual gas concentrations with partly unknown properties, Figs. 1 and 8 are in general rather similar. At least both of these plots can be used to the same extent for the separation of the Gaussians, arising most likely from the real HI emission from those probably caused by different observational and reductional problems and there is even no need to considerably change the selection criteria described above. In both figures we can also see similarities in the distribution of the Gaussians with realistic parameters: two main

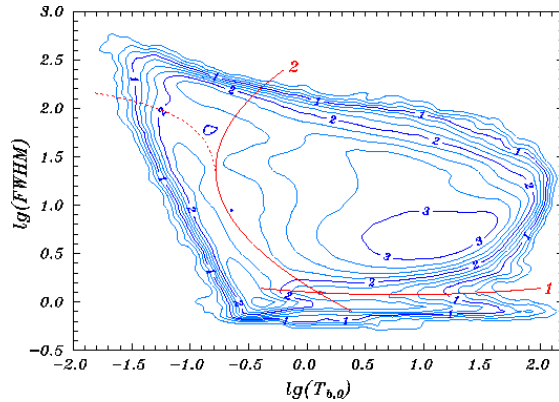


Fig. 8. Frequency distribution of the parameters of all Gaussians corresponding to profiles at galactic latitudes $|b| < 30^\circ$.

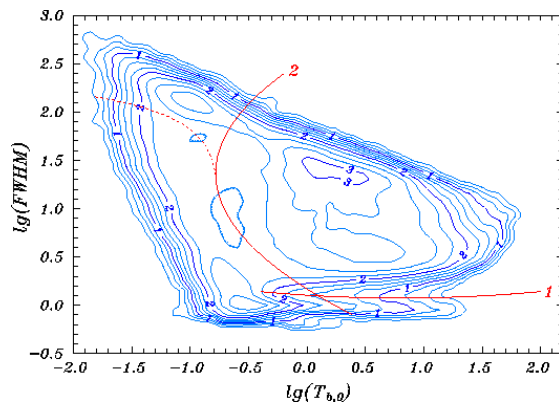


Fig. 9. The same as Fig. 1, but for the published version of the LDS. The plot is scaled to the same number of profiles as in Fig. 1.

concentrations in the width interval $3 < \text{FWHM} < 35 \text{ km s}^{-1}$. Therefore, it is possible to obtain from the near plane data at least some results similar to those obtainable at higher latitudes.

When for the testing of the decomposition program we used the original profiles as described above, it is also interesting to check how much the decomposition results are affected by the averaging of the re-observed profiles and by re-gridding of the whole survey. Therefore, in Fig. 9 we present as an example an analog of Fig. 1 for the published version of the LDS. We can see that this version of the plot is rather similar to that of Fig. 1. The most significant difference is that in the decomposition of the LDS Atlas data the resulting Gaussians are somewhat weaker than in the case of original profiles. This is best visible if we compare the locations of the distribution maximums around $\lg(T_{b0}) \approx 0.5$ and $\lg(\text{FWHM}) \approx 0.6$ in Figs. 1 and 9 and this may be explained as a result of interpolation between profiles with slightly differing locations of the line peaks – these peaks have been smoothed down. The decomposition of the Atlas data contains also larger numbers of weak Gaussians and the weakest components are weaker than in the case of the original LDS. However, this is a rather natural result, as both, re-gridding (interpolation) and averaging of the observed profiles reduce the mean noise level of the results and force the decomposition program to fit more weak Gaussians to the data.

The comparison of Figs. 1, 8 and 9 also illustrates the uncertainties of the selection criterion 2 for the widest Gaussians. When for widths $\lg(\text{FWHM}) \lesssim 1.35$ the line selected on the basis of Fig. 1 is more or less acceptable also for other cases, above this value for $|b| < 30^\circ$ the dashed line seems to be more acceptable and for the Atlas data both versions of the line 2 are rather arbitrary.

4. LAB

To cover the total sky, this compilation combines a revised version of the LDS with the IAR survey. We discuss the properties of both surveys individually.

4.1. LDS2

When discussing the results for the original version of the LDS, we identified in the (T_{b0}, FWHM) distribution three regions of the Gaussians, corresponding most likely to different problems, occurring during the observations and data reduction. These Gaussians represented the noise, radio-interferences, increased uncertainties near the profile edges and problems in baseline determination or in stray-radiation corrections. For the LDS2, included into the LAB, the stray-

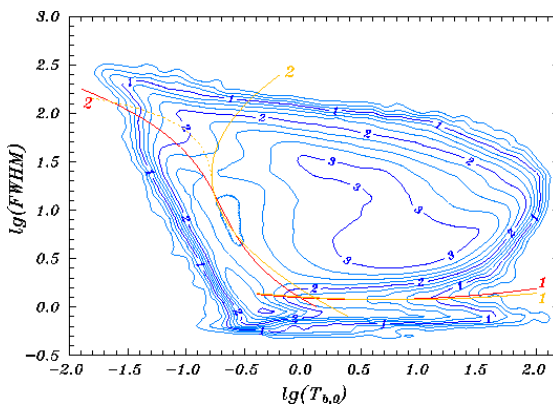


Fig. 10. The same as Fig. 1, but for all profiles of the LDS2. The selection criteria derived for the LDS are still indicated by solid and dashed orange lines, but those used for the LAB are in solid red lines.

radiation corrections and the baselines were recalculated (Kalberla et al. 2005) and therefore it is interesting to compare the decomposition results for the LDS and the LDS2. The (T_{b0}, FWHM) distribution of the Gaussians obtained from the decomposition of the LDS2 is given in Fig. 10. In this case, all the profiles of the survey are used for the plot and therefore it corresponds to the sum of the distributions given in Figs. 1 and 8. From the comparison of these distributions we can see that in the LDS2 the widest Gaussians obtained for the LDS are missing, but there are no considerable changes in other regions of problematic Gaussians. This may be considered as an indication that the recalculation of the stray-radiation corrections and baselines has improved the results.

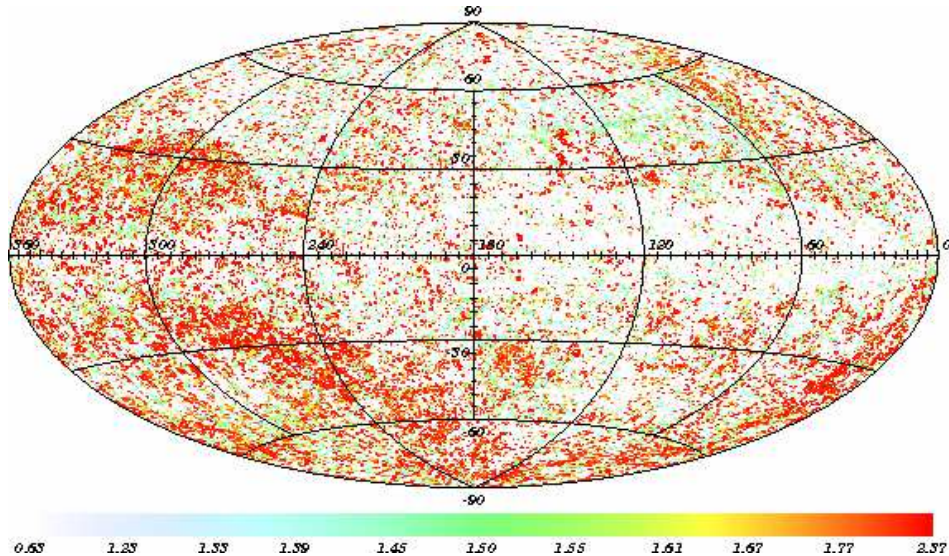


Fig. 11. The sky distribution of the widest weak Gaussians of the LDS2 in galactic coordinates. The color-scale represents the width (in units of $\lg(\text{FWHM})$) of the widest Gaussian obtained for a given sky position, and the gradation is chosen to enhance the contrast for the Southern sky.

To further check the situation with the wide Gaussians, we present in Fig. 11 for the LAB the distribution of the widest Gaussians in the sky. This picture is based on the same selection criteria as used for Fig. 6. Only, to stress some Southern sky features, the center of the color-scale is downshifted to $\lg(\text{FWHM}) = 1.5$, but this has no considerable effect on the appearance of the Northern sky. When compared to Fig. 6, it is obvious that the checkered pattern, which was so conspicuous in the case of the LDS has nearly disappeared in the LDS2, and therefore we may conclude that the stray-radiation corrections and base-line determinations for the LDS2 have been made at least much more homogeneously than for the LDS. Concerning Fig. 10, this also means that in the case of the upper part of the selection criterion 2 the solid line preferred for the LDS seems now rather obsolete and the dashed curve is a much more attractive choice. Therefore, at least on the basis of the distribution of the Gaussian parameters most of the weak wide components seem to correspond to some real population of galactic HI – most likely the HVDHG, discussed by Kalberla et al. (1998).

4.2. IAR

When we started the decomposition of the IAR, the first results were rather disappointing and surprising: on an average, we got per every profile about 1.65 times more Gaussians than in the case of the LDS or the LDS2 and most of these Gaussians were relatively narrow and weak. This was exactly the behavior that may be expected from the decomposition program, if the estimates of the noise level of the profiles are too low. In this case the program tries to reduce the rms of the residuals below the actual noise level of the survey and the only way to achieve this is to add into the decomposition many weak narrow components, which represent the strongest peaks of the observational noise. Therefore, we first checked our determination of the noise level in signal-free regions of the profiles. We used several different algorithms for estimating this noise level (they have been described in detail in Paper I) and concluded that the results of different methods agreed very well with each other and with the estimate for the final mean rms noise of the database given by Bajaja et al. (2005). From this we concluded that the problem cannot lie in the determination of the noise level of the signal-free parts of the profiles.

Another possibility was that the problems may hide in the usage of the radiometer equation for the description of the noise strength dependence on signal intensity. To get the first insight, we compared channel by channel the re-observed profiles (the detailed description of this procedure is given in Section 2.1. of Paper I). To reduce the role of uncertainties in the brightness temperature calibration and other possible scaling problems, we first compared the average channel values inside the usable velocity range of profiles at the same sky positions and rejected all results for the positions where the dispersion

of these averages for different profiles was more than 0.05 K (selecting even a smaller limit did not considerably change the results). Next we normalized all profiles at the same sky position to the same average channel value and compared all possible pairs of profiles at a given sky position channel by channel. In this comparison we used the average of corresponding channel values from different profiles as an indication of the signal level and their difference as an indication of the noise level. The results for small signal strengths are given with crosses in Fig. 12. We can see a rather unexpected behavior. Where the signal is missing, the results once again agree very well with the mean noise estimates for the survey. However, already for the 0.5 K signal the uncertainties in channel values

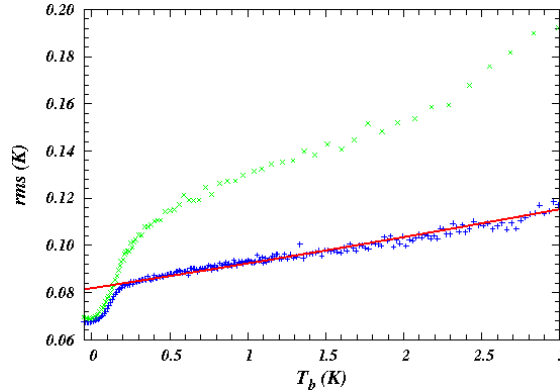


Fig. 12. The dependence of the total uncertainties (green crosses) in channel values and of the observational noise (blue pluses) on the signal strength. The thick solid red line indicates extrapolation of the noise level in regions containing the line emission into the signal-free region.

have increased nearly twice and only after this the uncertainties grow more or less linearly with the signal, as expected from the radiometer equation.

What is described above, is a rather direct estimation of the uncertainties in channel values at different levels of the signal. However these estimates contain not only observational noise, but they may also have been considerably increased by uncertainties in data reduction procedures (baseline, stray-radiation etc.). To study the pure noise, we must reject other sources of differences between the reobserved profiles. To some extent, this can be done by smoothing every profile and taking the smoothed version of the profile as an estimate of the signal behavior and the differences between original and smoothed versions as an estimate of the noise. For such smoothing we used the Savitzky-Golay filters of the second degree with different window widths. In Fig. 12 the plus signs show the results for (2,2,2) filter. Once again, the results for signal-free regions agree well with other estimates, but in the region of signal strengths of about 0.02 – 0.5 K there is a rapid increase in noise and only after this the noise behaves more or less as predicted by the radiometer equation. Of course, now the estimates of the noise strength in the regions containing a signal are considerably lower than those, obtained from the reobserved profiles, but these differences are in good agreement with the expectations by Bajaja et al. (2005) that “the necessary interpolation of the baseline leads to uncertainties which are enhanced by a factor of 2 to 3 over the typical rms uncertainties of 0.07 K as determined outside the regions with line emission”.

On the basis of the described results, we decided to slightly modify the noise estimates used in the decomposition program. We still obtain the main estimate of the noise strength from the signal-free regions of the profiles, but for regions with HI emission we allow for a 16% higher noise level. Such a model is indicated in Fig. 12 by the solid line. The 16% increase is chosen as a conservative value from the results with different smoothing filters. This estimate is not very precise, but we believe that the actual value cannot be considerably smaller, but according to some results may be even somewhat larger (up to about 21%). We also rechecked the LDS data for the presence of such a jump and found no need for introducing a similar correction in this case. After including the described 16% correction into the decomposition process of the IAR data, the results become much more similar to those of the LDS2. In the case of the IAR, there are still on an average 14% more Gaussians per profile than for the LDS2, but this may be natural, as there is also about 27% more HI per profile in the Southern sky than in the Northern sky.

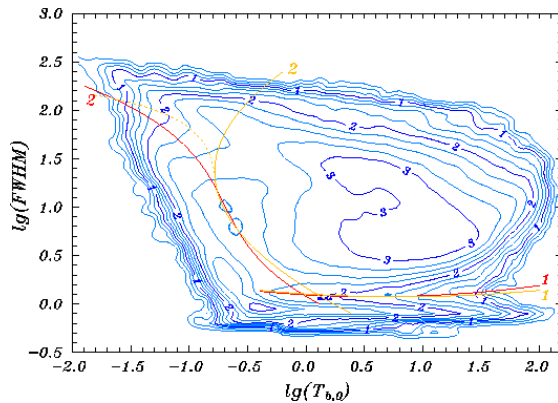


Fig. 13. The same as Fig. 10, but for the IAR. The plot is scaled to the same number of profiles as in Fig. 10.

The (T_{b0}, FWHM) distribution of the Gaussians obtained from the decomposition of the IAR is given in Fig. 13. When comparing with Fig. 10, we can see that now the numbers of weak narrow Gaussians are in both cases rather similar, but for the IAR there are more strong narrow Gaussians than in the case of the LDS2. Most likely these are the interference induced profile components mentioned also by Bajaja et al. (2005). Due to the larger number of Gaussians per profile in the Southern sky the overall extent of the distribution in Fig. 13 is also wider than in Fig. 10, but the general shapes of the isolines are rather similar, except in the region $-1.0 \lesssim \lg(T_{b0}) \lesssim -0.5$ and $1.5 \lesssim \lg(\text{FWHM}) \lesssim 2.0$, where the IAR seems to contain considerably more Gaussians than the LDS2. This is visible also from Fig. 10, where the Southern sky shows once again the quadrangular patterns discussed in connection with the baseline problems of the LDS and mentioned also by Bajaja et al. (2005). However, in this case the quadrangular pattern is visible in narrower Gaussians than in the LDS, indicating that in the IAR at least some baseline defects are smaller in their frequency extent (Fig. 14).

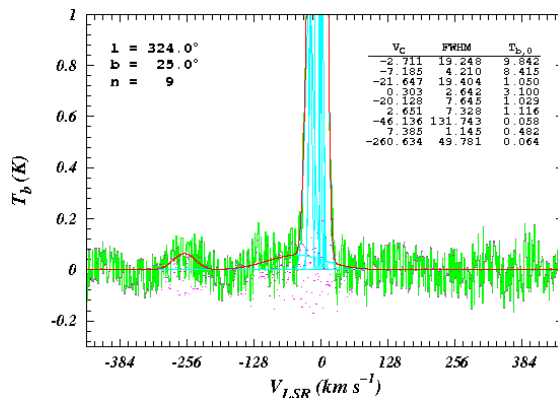


Fig. 14. An example of the IAR profile with bad base-line. The notation is the same as in Fig. 2.

5. CONCLUSIONS

In this paper we have mainly used the high galactic latitude part $|b| \geq 30^\circ$ of the Leiden/Dwingeloo Survey of galactic neutral hydrogen by Hartmann & Burton (1997) to demonstrate how the Gaussian analysis could be used for statistical cleaning of the observed H I profiles from observational noise and different observational and reductional artifacts. The removal of most of the observational noise is achieved by the process of the Gaussian decomposition. The program searches in profiles the regions where the measured brightness temperatures are above the estimated noise level, and fits this excess with the Gaussian function of three free parameters. The Gaussians are added until the rms of the residuals becomes close to the initial noise level estimate of the signal-free regions of the profile (the detailed description of the decomposition process is given by Haud 2000). At this point the residuals are considered as pure observational noise and discarded from further consideration.

We have demonstrated that not all Gaussians obtained in this way could be considered as representing the real H I emission of the Milky Way. A considerable part of the obtained Gaussians are still due to different observational, reductional and decompositional problems, which have occurred during this process. However, we have demonstrated that by analyzing the distribution of the parameters of the obtained Gaussians, it is possible to further clean the results by distinguishing

the components, modeling different artifacts from those representing the actual emission of the galactic hydrogen. Such a separation is easy for very narrow Gaussians, which represent the radio-interferences not found and removed during the reduction of the observed profiles, and the strongest random noise peaks misinterpreted by the decomposition program as possible signal peaks. Disregarding such Gaussians seems to be possible on the basis of their location in the line-width – intensity distribution alone.

A considerable amount of somewhat wider weak Gaussians seem to be caused by the increased uncertainties in bandpass removal near the profile edges. In the direction of wider Gaussians this region smoothly transforms to the one dominated by Gaussians, most likely representing problems in the determination of the baselines of the profiles. As demonstrated by Fig. 3, at these widths our criterion based on line-widths and heights alone, becomes somewhat unreliable. There are considerable numbers of components with heights larger than allowed by our selection criterion, but still most likely not representing the real HI emission. However, these Gaussians could easily be recognized from their velocities. These are the Gaussians with central velocities lying outside the velocity limits of the profile, actually used during the Gaussian decomposition. They are the components, modeling the cases of rising profile edges and their intensities are estimated from the small number of profile channels covering only the minor part of the region, where the corresponding Gaussian has considerable intensities.

In the LDS the region of the widest weak Gaussians is most likely dominated by the baseline problems, but when dealing with these components their velocity information must also be considered as in the regions $-390 < V_C < -230 \text{ km s}^{-1}$ and $180 < V_C < 280 \text{ km s}^{-1}$ the selection criterion based on the line-widths and heights alone will discard also some information about HVCs. At the level of the present discussion it remains unclear, if and how Gaussians represent the high velocity dispersion halo gas reported by Kalberla et al. (1998). On the basis of the data presented in their paper, it seems that our selection criteria for the LDS discard most of this gas as well. At the same time, it seems to be impossible to decide on the basis of the single profile data, whether it contains the emission from HVDHG or a baseline problem.

It is well known that near the galactic plane the HI 21-cm emission line profiles are so complicated that it is impossible to derive from the Gaussian analysis reliable conclusions on physical properties of the gas concentrations. Nevertheless, the comparison of Figs. 1 and 8 demonstrates that at least the selection criteria for discarding different artifacts are applicable in both cases without modifications. Moreover, despite clear differences in the distributions of the parameter values of the Gaussians, representing the HI emission for regions $|b| \geq 30^\circ$ and $|b| < 30^\circ$, there are still some similarities, indicating that at least for some profiles in the region $|b| < 30^\circ$ not all of the useful information may be completely "washed out" by velocity crowding, blending and other effects.

The approach used for the LDS is applied also to the new LAB, where we may conclude that the baseline estimates for the LDS2 part of the LAB have been made considerably more uniform, if compared to the LDS (the conspicuous "chess-board" sky has disappeared), but for the IAR the baseline may still be somewhat questionable. Also, the problems caused by radio-interferences may be more severe in the case of the IAR than for the LDS2. Moreover, we point out the strange behavior of the observational noise in the IAR, where only the estimates

for signal-free regions are in agreement with those, published by the authors of the survey. The behavior of the noise in the regions with line emission corresponds to the one expected on the basis of the radiometer equation only if we accept that the rms in these regions is about 15 – 21% higher than the estimate derived from the emission-free regions. Only after taking into account such behavior of the noise estimates, it is possible to obtain for the IAR the decomposition results similar to those of the LDS or the LDS2.

When comparing the shapes of the distributions of Gaussian parameters for different version of the surveys, we may conclude that for most cases the selection criteria for separation of the components, most likely not related to the emission of galactic H I, are rather universal. The only exception is the region of the widest Gaussians, which in the case of the LDS seems to be dominated by the components caused by the badly defined baseline, but the situation may be different for the LAB. Therefore, considering also the uncertainties in the determination of the selection criteria, those based on the LDS and given by Eqs. (2) and (3), are to some extent applicable also to the LAB. However, mostly due to the differences in the situation with the widest Gaussians, those indicated in Figs. 10 and 13 with solid red lines are preferred for the LAB. Corresponding functional expressions are:

$$\lg(\text{FWHM}) = 0.057 * \lg(T_{b0})^2 - 0.067 * \lg(T_{b0}) + 0.094 \quad (4)$$

for line 1 and

$$\lg(T_{b0}) = -0.370 * \lg(\text{FWHM})^3 + 1.132 * \lg(\text{FWHM})^2 - 1.567 * \lg(\text{FWHM}) + 0.117 \quad (5)$$

for line 2 respectively. These criteria are selected on the basis of the full LAB data (the LDS2 and the IAR combined). Eq. (4) may be applied irrespective of the velocities of the Gaussians involved, but Eq. (5) seems to be useful mainly for the relatively slow components in the velocity interval of about $|V_C| \lesssim 150 \text{ km s}^{-1}$. At higher velocities the parameters of the Gaussians, describing the HVCs, some external galaxies and the survey artifacts may be rather similar and it is hard to decide on the basis of these parameters alone, what may be the actual source of the corresponding Gaussian. Eq. (5) becomes also important at the extreme velocities near the profile edges where the probability of spurious components increases. The Gaussians with the central velocities outside the velocity range, used for the decomposition, must also be excluded as due to the uncertainties introduced by the bandpass removal.

Finally, we would like to stress that all the discussion in this paper is statistical in its nature and the selection criteria presented could not be taken as a final truth for every particular profile and Gaussian component. As we hope, these criteria permit us to detect and reject most of the problematic cases described above and in this way to reduce the number of the undesirable components in the database. However, there are certainly cases, not detected by these criteria and also cases where important astrophysical signatures may be removed. Therefore, in the first order these criteria are useful for statistical work on the Milky Way H I. However, they can also be used as first guiding lines for labeling the problematic profiles in the surveys. For example, in the case of multiple observations at the same position of the LDS2, the criteria described above have been used to select the "best" profile which is expected to be the least problematic in the sense of the presence of spurious features discussed in this paper. However, the final decision

on the nature of such features must be made on the basis of the inspection of the actual profiles and other astronomical observations.

ACKNOWLEDGEMENTS. We would like to thank W. B. Burton for providing the preliminary data from the LDS for testing the decomposition program prior the publication of the survey. We are also grateful to him for serving as a referee of this paper and for valuable discussions. A considerable part of the work on creating the decomposition program was done during the stay of U. Haud at the Radioastronomical Institute of Bonn University. The hospitality of the staff members of the Institute is greatly appreciated. We are thankful to E. Saar and J. Pelt for valuable suggestions and discussions. The project was supported by the Estonian Science Foundation grant no. 6106.

REFERENCES

- Bajaja E., Arnal E. M., Larrarte J. J., Morras R., Pöppel W. G. L., Kalberla P. M. W. 2005, *A&A*, 440, 767
- Baker P. L., Burton W. B. 1979, *A&AS*, 35, 129
- Braun R., Burton W. B. 2000, *A&A*354, 853
- Burton W. B. 1966, *BAN* 18, 247
- Burton W. B. 1992, in *The Galactic Interstellar Medium*, ed. D. Pfenniger & P. Bartholdi, Saas-Fee Advanced Course 21, 1
- Cappa de Nicolau C. E., Pöppel W. G. L., 1986, *A&A*164, 274
- Crovisier J. 1981, *A&A*, 94, 162
- Dickey J. M., Lockman F. J. 1990, *ARA&A*, 28, 215
- Field G. B., Goldsmith D. W., Habing H. J., 1969, *ApJ*, 155, L149
- Hartmann L. 1994, *The Leiden/Dwingeloo Survey of Galactic Neutral Hydrogen*, Ph. D.-Thesis, Leiden Univ
- Hartmann L., Burton W. B. 1997, *Atlas of Galactic Neutral Hydrogen*, Cambridge Univ. Press, 10+236 pp
- Hartmann L., Kalberla P. M. W., Burton W. B., Mebold U. 1996, *A&AS*, 119, 115
- Haud U. 2000, *A&A*, 364, 83
- Kalberla P. M. W., Westphalen G., Mebold U., Hartmann D., Burton W. B. 1998, *A&A*, 332, L61
- Kalberla P. M. W., Burton W. B., Hartmann D., Arnal E. M., Bajaja E., Morras R., Pöppel W. G. L. 2005, *A&A*, 440, 775
- Kaper H. G., Smits D. W., Schwarz U., Takakubo K., van Woerden H. 1966, *BAN* 18, 465
- Kulkarni S. R., Fich M. 1985, *ApJ*, 289, 792
- Kulkarni S. R., Heiles C. 1987, in *Interstellar Processes*, ed. D. Hollenbach & H. A. Thronson, Jr. (Dordrecht: Reidel), 87
- Mebold U. 1972, *A&A*, 19, 13

- Mebold U., Winnberg A., Kalberla P. M. W., Goss W. M. 1982, *A&A*, 115, 223
Pöppel W. G. L., Marronetti P., Benaglia P. 1994, *A&A*, 287, 601
Shane W. W. 1971, Observations of Neutral Hydrogen in an Interior Region of the Galaxy and the Structure and Kinematics of the Scutum Spiral Arm, Ph. D.-Thesis, Leiden Univ
Takakubo K., van Woerden H. 1966, *BAN*, 18, 488
Verschuur G. L., Knapp G. R. 1971, *AJ*, 76, 403
Verschuur G. L., Knapp G. R. 1972, *AJ*, 77, 717
Verschuur G. L., Schmelz J. T. 1989, *AJ*, 98, 267
Verschuur G. L., Magnani L. 1994, *AJ*, 107, 287
Verschuur G. L., Peratt A. L. 1999, *AJ*, 118, 1252
Verschuur G. L. 2004, *AJ*, 127, 394